An ab Initio Study of Solid Nitromethane, HMX, RDX, and CL20: Successes and Failures of DFT

Edward F. C. Byrd,* Gustavo E. Scuseria,† and Cary F. Chabalowski‡

US Army Research Laboratory, AMSRL-WM-BD, APG, Maryland 21005-5066, Department of Chemistry, Rice University, MDAB 310, Houston, Texas 77251-1892, and SAAL-TT, 2511 Jefferson Davis Highway, Suite 9000, Arlington, Virginia 22202-3911

Received: March 24, 2004; In Final Form: June 29, 2004

Using the PW91 and PBE density functional theories (DFT), we have studied four energetic molecular crystals, nitromethane, HMX, RDX, and CL20, with a wide range of basis sets. Intramolecular distances, simple angles, and band gaps are converged at plane wave cutoff energies (E_{cut}) of 430 to 495 eV. Cell parameters were determined over a range of E_{cut} values from 280 eV to 700 or 800 eV, depending upon the system. Lattice vectors, however, display large errors in the range of 0.2 Å to 1.0 Å (up to a 9.6% error at the highest E_{cut} used here), and a very slow convergence on basis set size. We hypothesize that the error in the lattice vectors is due to a lack of van der Waals forces in current DFT functionals. This deficiency will have unforeseen consequences on all crystal calculations for organic molecules, and therefore caution should be employed whenever interpreting results obtained from the current DFT functionals available in solid state codes. To properly describe the electronic structure of these types of crystals, these results suggest the need for new methods involving DFT to be developed which include accurate dispersion forces.

1. Introduction

Recent advances in density functional theory (DFT)[1] have allowed the study of large polyatomic molecules and crystals. These advancements have become part of the standard set of tools used in the development and evaluation of energetic materials. Density functional theories exhibit reasonable accuracies coupled with computational efficiency, and for such reasons they have been used to study, both statically and dynamically, large molecular systems. Previous work for energetic species utilizing density functional theories has ranged from gas phase structure studies of RDX[2] to shocked nitromethane calculations.[3,4] Density functional theory has also been used in the charting of the unimolecular decomposition pathways for both RDX[5] and HMX.[6]

Inspired by the work of Reed et al.,[3] we initially desired to examine the possibility of band gap lowering under compression as a mechanism for detonation, as proposed by Kuklja et al.[7] However, upon testing for basis set convergence, we realized there were significant errors present in the lattice vectors when using density functional theories. These errors in the lattice vectors can translate into large errors in the computed crystalline densities of these energetic molecular crystals.

The density of crystalline energetic materials is considered to be one of the primary physical parameters in detonation performance, since detonation velocities and pressures of energetic materials are proportional to powers in the density. Currently, most density predictions are within 2−4% of experimental values, depending on the class of compounds. Experimentalists would prefer predictions with deviations of 1% or less.[8] Thus, any calculations that yield computed densities with errors greater than 4−5% are undesirable. In this paper, we shall demonstrate that current formulations of DFT are unsuitable for predictions of densities of energetic molecular crystals at ambient conditions, and we shall quantify the errors one can expect from density functional theory.

2. Computational Details

Calculations of the crystal parameters and intramolecular bond distances and angles for nitromethane (NO_2CH_3), 1,3,5,7-tetranitro-1,3,5,7-tetraazacyclooctane (HMX), cyclotrimethylenetrinitramine (RDX), and 2,4,6,8,10,12-hexanitrohexaazaisowurzitane (CL20) were done using the generalized gradient approximation density functional theory (GGA DFT) Perdew−Wang 91 (PW91)[9] functional as implemented in the Vienna Ab-Initio Package (VASP).[10] The Perdew−Burke−Ernzerhof (PBE)[11] functional was also employed as an alternate method for nitromethane and RDX. The Vanderbilt ultrasoft pseudopotentials (USP)[12] and Monkhorst−Pack *k*-point generation method were used for all calculations. Plane wave kinetic energy cutoffs (E_{cut}) ranged from 280 eV to 800 eV.

Starting from experimental crystal structures, all ionic and cell degrees of freedom were allowed to relax concurrently and without enforcement of symmetry restrictions. Theoretical equilibrium crystal structures were obtained through analytic gradient techniques. The electronic energies were converged to 2.0×10^{-6} eV, while the structures were converged once the difference in free energy between gradient steps was less than 2.0×10^{-5} eV. As these molecular crystals are insulators, setting the smearing width to 0.0001 in the Methfessel−Paxton method[13] minimized electron smearing. To accelerate convergence, the RMM-DIIS method was employed, except for certain calculations where it was necessary to use conjugate gradients instead.

As a comparison of plane wave versus Gaussian basis set calculations, we obtained calculations of nitromethane using the

* Author to whom correspondence should be addressed. US Army Research Laboratory. Tel: 410-306-0729. E-mail: ebyrd@arl.army.mil.
† Rice University. Tel: 713-348-4746. E-mail: guscus@rice.edu.
‡ SAAL-TT. Tel: 703-604-7445. E-mail: cary.chabalowski@saalt.army.mil.

10.1021/jp0486797 CCC: $27.50
Published on Web 08/10/2004

TABLE 1: Mean, Percent Mean, Absolute Mean, Standard Deviation, and Maximum Error in Intramolecular Bond Distances versus Experiment for Various Kinetic Energy Cutoffs for the Nitromethane Crystal with PW91

E_{cut} (eV)	mean (Å)	% mean	abs mean (Å)	std dev (Å)	max error (Å)
280	0.0063	0.0630	0.0190	0.0231	0.037
330	0.0115	1.0309	0.0172	0.0182	0.038
380	0.0135	1.1824	0.0158	0.0155	0.037
430	0.0155	1.3325	0.0158	0.0136	0.037
495	0.0167	1.4239	0.0167	0.0128	0.037
545	0.0167	1.4239	0.0167	0.0128	0.037
645	0.0168	1.4352	0.0168	0.0126	0.037
700	0.0167	1.4237	0.0167	0.0125	0.037

TABLE 2: Mean, Percent Mean, Absolute Mean, Standard Deviation, and Maximum Error in Intramolecular Angles versus Experiment for Various Kinetic Energy Cutoffs for the Nitromethane Crystal with PW91

E_{cut} (eV)	mean (deg)	% mean	abs mean (deg)	std dev (deg)	max error (deg)
280	0.0333	0.0548	1.5444	2.1319	4.5
330	0.0222	0.0422	1.3556	1.9942	4.2
380	0.0111	0.0318	1.3000	1.8878	3.9
430	0.0111	0.0299	1.3000	1.8128	3.7
495	0.0111	0.0300	1.3000	1.8114	3.7
545	0.0222	0.0376	1.3111	1.7513	3.4
645	0.0333	0.0484	1.3444	1.8104	3.6
700	0.0222	0.0392	1.1068	1.7957	3.6

Guassian03 (G03) solid state package.[14] Two calculations were performed using the 3-21G and 6-31G** basis sets.[15]

3. Results and Discussion

3.1. Nitromethane. The simplest of the four energetic materials studied is nitromethane, with four molecules contained in the primitive cell. The space group is $P2_12_12_1$ with 28 atoms in the cell and experimental lattice vectors (taken at 4.2 K) of **a** = 5.183 Å, **b** = 6.236 Å, and **c** = 8.518 Å and lattice angles of $\alpha = \beta = \gamma = 90.0°$.[16] We tested for an appropriate *k*-point grid by running calculations at a kinetic energy cutoff of 545 eV with one (1 × 1 × 1), four (2 × 2 × 2), fourteen (3 × 3 × 3), and thirty-two (4 × 4 × 4) *k*-points with the PW91 functional. The difference in lattice vectors between the four and thirty-two *k*-point grids was at most −0.007 Å (−0.118%). Therefore, the remainder of the calculations were performed using a four *k*-points grid. In testing for convergence with kinetic energy cutoff, we ran calculations at 280, 330, 380, 430, 495, 545, 645, and 700 eV with the PW91 functional.

Inspecting first the intramolecular bond distance errors versus experiment in Table 1, we see by an E_{cut} of 495 eV, the errors have converged to very acceptable values. With an absolute mean of only 0.017 Å and a standard deviation of 0.013 Å by 495 eV, we see an excellent agreement with experiment. The largest error for nitromethane is one of the nitrogen−oxygen bonds, with every kinetic energy cutoff consistently resulting in a 0.04 Å error. The PW91 functional yields approximately the same bond lengths for each of the nitrogen−oxygen bonds, while the experimental lengths of the N−O bond differ (1.209 Å and 1.223 Å). This error in the N−O bond length is not carried over into the angles (Table 2), where it is one of the methyl hydrogens that yields the largest error of approximately 3.6° relative to the nitrogen. Outside of this lone case, the other angles do not exhibit any error to experiment greater than 3° and are for the most part well-behaved.

Turning now to the crystal lattice parameters, we see a disturbing trend in the error to experiment versus the kinetic energy cutoff. Figure 1 illustrates how, at high E_{cut}, the percent error to experiment is fairly large, with a maximum percent error of 8.5% (0.53 Å) for the **b** lattice vector at 545 eV. While the negative errors seen for the small E_{cut} are also large, this is understandable as there are far too few plane waves at these low E_{cut} to properly describe the momentum space. However, at larger E_{cut} values, the convergence of the **b** lattice vector to approximately 7% error even at a large E_{cut} is indicative that the current implementation of DFT is unsuited to molecular crystalline compounds. We shall see similar trends in the other molecular crystals in this study.

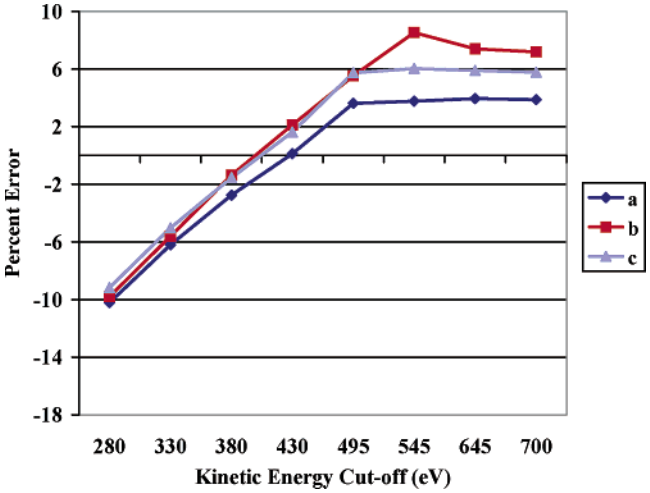

Figure 1. PW91 percent errors versus experimental lattice vectors for nitromethane.

A possible source of error for these calculations is that VASP keeps the number of plane waves in the calculation constant, regardless of change in cell volume. To be certain that we properly saturated the momentum space with plane waves and that increasing the cell volume will not cause a Pulay stress error, we started a new cell convergence calculation from the converged geometry at 545 eV without changing any parameters. Upon completion, the largest change in lattice vector was −0.024 Å (−0.47%) for the **a** lattice vector. This minimal change allows us to state that at the higher E_{cut} the momentum space is adequately described and that Pulay stresses are not a concern.

Other possible sources of error would be errors inherent to the PW91 functional or the plane wave basis sets. We therefore computed the crystalline dimensions using the VASP implemented PBE functional with a four *k*-point grid and with the 495, 545, and 645 eV basis sets. We also determined the lattice vectors using the 3-21G and 6-31G** Gaussian basis sets with the G03 implemented PBE functional. Figure 2 illustrates the errors in the **a**, **b**, and **c** lattice vectors for the above methods and functionals, as well as with the PW91 functional using the 495, 545, and 645 eV basis sets for comparison.

The plane wave PBE functional yields errors approximately 0.5−1.0% lower than the PW91 functional, with a few exceptions. For the **b** lattice vector, PW91 at 545 eV has larger errors than the PBE functional, while the reverse holds true for the 645 eV basis set. The PBE functional does not seem to dramatically improve upon the results found with the PW91 functional.

For the Gaussian basis sets, it is readily apparent the 3-21G basis set is too small to properly describe the nitromethane crystal. The 6-31G** basis set, however, does reasonably well for the **a** and **c** lattice vectors, but shows a 4.96% error in the **b** lattice length. It seems the Gaussian basis sets display similar

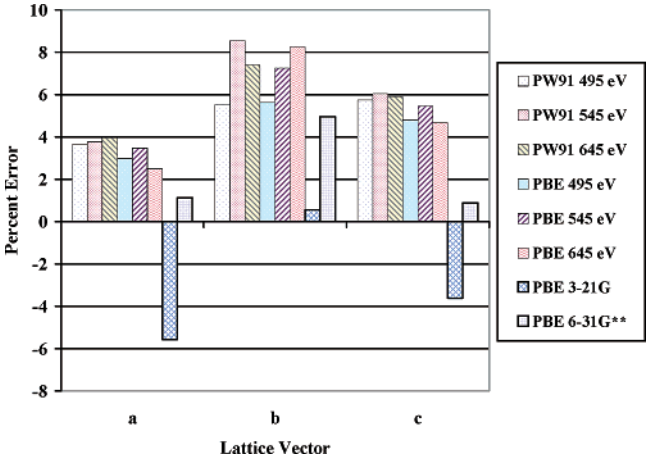

Figure 2. Percent errors versus experimental lattice vectors for nitromethane.

TABLE 3: Mean, Percent Mean, Absolute Mean, Standard Deviation, and Maximum Error in Intramolecular Bond Distances versus Experiment for Various Kinetic Energy Cutoffs for the β-HMX Crystal with PW91

E_{cut} (eV)	mean (Å)	% mean	abs mean (Å)	std dev (Å)	max error (Å)
280	−0.0031	−0.1911	0.0195	0.0229	0.045
330	0.0035	0.2973	0.0135	0.0190	0.044
380	0.0074	0.5782	0.0116	0.0164	0.041
430	0.0091	0.7080	0.0125	0.0156	0.039
495	0.0104	0.7994	0.0136	0.0154	0.038
545	0.0104	0.8056	0.0137	0.0153	0.037
700	0.0104	0.8047	0.0137	0.0154	0.038

TABLE 4: Mean, Percent Mean, Absolute Mean, Standard Deviation, and Maximum Error in Intramolecular Angles versus Experiment for Various Kinetic Energy Cutoffs for the β-HMX Crystal with PW91

E_{cut} (eV)	mean (deg)	% mean	abs mean (deg)	std dev (deg)	max error (deg)
280	−0.0400	−0.0233	0.8880	1.3150	3.3
330	0.0760	0.0763	0.7400	1.1107	2.6
380	0.0640	0.0663	0.7280	1.0618	2.6
430	0.0600	0.0600	0.7960	1.0851	−2.6
495	0.0760	0.0731	0.8520	1.1092	−2.7
545	0.0800	0.0764	0.8720	1.1273	−2.8
700	0.0520	0.0523	0.8200	1.0978	−2.8

trends in the errors as the plane wave basis sets, and as the results should be independent of the nature of the basis set employed, this was not unexpected.

3.2. HMX. We look next to β-HMX, the most stable polymorph of HMX, which exhibits a space group of $P2_1/c$ with 56 atoms in the unit cell and experimental lattice vectors of **a** = 6.54 Å, **b** = 11.05 Å, and **c** = 8.7 Å and lattice angles of $\alpha = \gamma = 90.0°$ and $\beta = 124.3°$.[17] We tested for an appropriate *k*-point grid by running calculations at a kinetic energy cutoff of 545 eV with two (2 × 1 × 2) and thirty-two (4 × 4 × 4) *k*-points. The largest difference in lattice vectors between the two different *k*-point grids was 0.009 Å (0.078%). Therefore the calculations for this study were performed using the two (2 × 1 × 2) *k*-point grid. In testing for convergence with kinetic energy cutoff, we ran calculations at 280, 330, 380, 430, 495, 545, and 700 eV.

As one can see in Tables 3 and 4, HMX follows a similar trend as nitromethane, where by an E_{cut} of 495 eV the errors have converged. We see a convergence to an absolute mean error of 0.014 Å (0.8% mean error) in bond lengths and a standard deviation convergence to 0.015 Å compared to

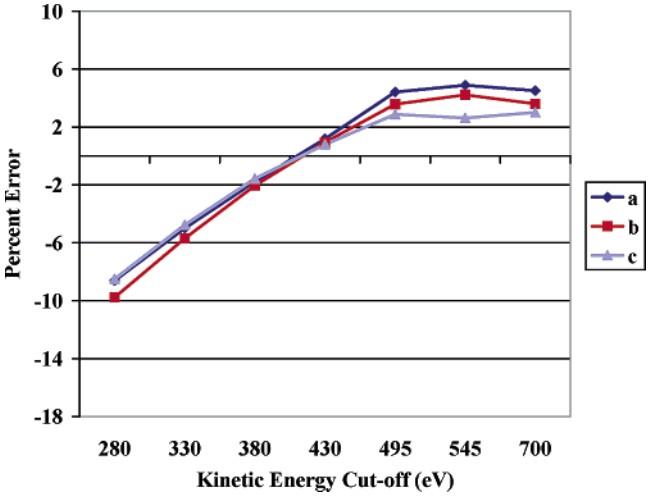

Figure 3. PW91 percent errors versus experimental lattice vectors for HMX.

experiment. The bond that displays the largest theoretical error is a nitrogen−oxygen bond off an axial NO_2 group. However, both N−O bonds of the axial NO_2 groups and one N−O bond of the equatorial NO_2 groups display errors of approximately 0.03 Å. No other bond exhibits errors larger than 0.019 Å in any E_{cut} after 280 eV, which, as stated in the previous section, is an unsuitable E_{cut} for molecular crystal calculations. All bond angles are within ±3° of experiment for all values of E_{cut} (Table 4).

In Figure 3, one sees that the percent errors in the lattice vectors increases as the E_{cut} values increase. Similarly to nitromethane, below 430 eV the lattice vectors are all shorter than experiment, while for 430 eV and above the percent errors were positive and growing with increasing E_{cut}. However, unlike nitromethane, all the lattice vectors appear to begin converging by 495 eV. The percent errors are also not as large as those seen in nitromethane, ranging from approximately 3% for the **c** vector to 5% for the **a** vector at an E_{cut} of 700 eV. The percent error in the β lattice angle shows no pattern and is consistently small, with most errors under 0.34°, with the exception of −1.5° at 545 eV. For this molecular crystal, both the intramolecular errors and the lattice vector errors seem to be converged by 495 eV. We shall see that these are the best results for DFT within the sample set of four molecular crystals in this study.

3.3. RDX. Examining next RDX, we are fortunate enough to have experimental gas phase data to compare against. In comparing to gas phase data, we will be able to gauge the accuracy of the theory with respect to plane waves and pseudopotentials. As there also exist previous theoretical calculations on the gas phase data using atomic orbitals, we will compare to these results as well.

As VASP was designed to compute periodic systems, to approximate gas phase conditions we ran an "isolated" molecule in a 15 × 15 × 15 Å^3 box with one *k*-point. Although this cell is replicated in all three spatial dimensions, the large vacuum around each molecule should be sufficient to eliminate any forces felt from its neighbors. Calculations were done using kinetic energy cutoffs of 280, 380, and 495 eV, and all calculations were started using the gas phase experimental structure as the initial geometry.

Comparing to the theoretical work done previously by Rice and Chabalowski (Tables 5 and 6),[2] we see that by 380 eV, PW91 with plane waves yields similar results to MP2/6-31G*. There is little improvement in going to a larger E_{cut}, as the results have converged by 380 eV. B3LYP with a Gaussian basis set,

TABLE 5: Mean, Percent Mean, Absolute Mean, Standard Deviation, and Maximum Error in Bond Distances versus Experiment for PW91, MP2, and B3LYP for the Gas Phase RDX Molecule

	mean (Å)	% mean	abs mean (Å)	std dev (Å)	max error (Å)
PW91 (280 eV)	0.0279	2.2232	0.0282	0.0220	0.070
PW91 (380 eV)	0.0186	1.5197	0.0205	0.0171	0.045
PW91 (495 eV)	0.0181	1.4860	0.0201	0.0171	0.045
MP2/6-31G* [a]	0.0184	1.4673	0.0197	0.0180	0.060
B3LYP/6-31G* [a]	0.0146	1.1558	0.0166	0.0160	0.051
B3LYP/6-311+G** [a]	0.0128	0.9965	0.0156	0.0171	0.054

[a] Reference 2.

TABLE 6: Mean, Percent Mean, Absolute Mean, Standard Deviation, and Maximum Error in Intramolecular Angles versus Experiment for PW91, MP2, and B3LYP for the Gas Phase RDX Molecule

	mean (deg)	% mean	abs mean (deg)	std dev (deg)	max error (deg)
PW91 (280 eV)	−0.0306	−0.0306	0.9750	1.1181	2.2
PW91 (380 eV)	0.2056	0.1739	0.8722	1.0450	2.3
PW91 (495 eV)	0.2194	0.1863	0.9306	1.0828	2.2
MP2/6-31G*	−0.8367	−0.7110	0.1459	1.9304	−7.25
B3LYP/6-31G*	−0.2794	−0.2352	1.0506	1.5470	−5.81
B3LYP/6-311+G**	0.2292	−0.1928	0.9897	1.4470	−5.48

however, displays a 0.0035 Å decrease in absolute mean error with the 6-31G* basis set versus PW91 with a 495 eV E_{cut}. There is marginal improvement in the errors for B3LYP in going to the larger 6-311+G** basis set, decreasing the absolute mean error by only an additional 0.001 Å. The bond with the largest error for all methods and basis sets compared to gas phase data (except for PW91 at 280 eV) is the equatorial nitrogen−nitrogen bond. The accuracy of these results validates the use of ultrasoft pseudopotentials, as they are sufficient to describe the intramolecular structure of organic species. These results also indicate that for accurate structures one does not need very high kinetic energy cutoffs for intramolecular distances. We have already seen evidence of this for the nitromethane and HMX molecular crystals. As we shall continue to demonstrate, however, the crystal lattice vectors are very sensitive to the level of E_{cut} chosen.

We examine next the crystal phase of α-RDX, the room temperature polymorph of crystalline RDX, containing 168 atoms per cell and with a space group of *Pbca* and experimental lattice vectors of **a** = 13.182 Å, **b** = 11.574 Å, and **c** = 10.709 Å and lattice angles of $\alpha = \beta = \gamma = 90.0°$.[18] *k*-Point testing was performed using the one (1 × 1 × 1) and four (2 × 2 × 2) *k*-point grids at 495 eV. The largest absolute difference in lattice vectors between the two different *k*-point grids was the **c** vector at 0.15 Å (1.4%) and the smallest difference the **a** vector at 0.02 Å (0.17%), with the four *k*-point grid yielding a longer **a** lattice vector but a shorter **c** vector compared to the one *k*-point grid. As the **c** vector still exhibits a large percent error of 7.78% with the four *k*-point grid, coupled with the size of unit cell, extensive calculations with the four *k*-point grid were not computationally feasible, and therefore the calculations were performed using the one (1 × 1 × 1) *k*-point grid. In testing for convergence with kinetic energy cutoff, we ran calculations at 280, 330, 380, 430, 495, 545, 700, and 800 eV.

In general the statistical errors versus experiment for RDX are slightly better in the crystal phase than in the gas phase. Absolute means have converged to 0.018 Å (1.4 mean % error) in the crystal phase, an improvement of 0.002 Å over the gas phase predictions (Table 7). The bond with the largest error varies with E_{cut} for this molecular crystal. For 330 and 380 eV, an axial N−O is the longest bond, while for 430 through 800 eV the short C−H bond (1.059 Å in experiment) yields the largest error versus experiment, as theory predicts all C−H bonds to be approximately the same length (∼1.09 Å). Generally, all N−O bonds are too long and have errors on the order of 0.04 Å, whether they are axial or equatorial NO_2 groups. For E_{cut} larger than 380 eV, almost all bonds are longer than experimental values and have converged to the same value by 430 eV.

TABLE 7: Mean, Percent Mean, Absolute Mean, Standard Deviation, and Maximum Error in Intramolecular Bond Distances versus Experiment for Various Kinetic Energy Cutoffs for the RDX Crystal with PW91

E_{cut} (eV)	mean (Å)	% mean	abs mean (Å)	std dev (Å)	max error (Å)
280	−0.0058	−0.3029	0.0256	0.0292	−0.047
330	0.0058	0.5679	0.0173	0.0217	0.041
380	0.0139	1.1729	0.0155	0.0160	0.041
430	0.0158	1.309	0.0170	0.0146	0.040
495	0.0166	1.3702	0.0175	0.0144	0.040
545	0.0167	1.3780	0.0178	0.0145	0.041
700	0.0165	1.3619	0.0175	0.0148	0.040
800	0.0167	1.3794	0.0177	0.0146	0.041

TABLE 8: Mean, Percent Mean, Absolute Mean, Standard Deviation, and Maximum Error in Intramolecular Angles versus Experiment for Various Kinetic Energy Cutoffs for the RDX Crystal with PW91

E_{cut} (eV)	mean (deg)	% mean	abs mean (deg)	std dev (deg)	max error (deg)
280	0.0917	0.0898	1.4472	2.0136	5.0
330	0.1778	0.1582	0.9278	1.1931	3.4
380	0.1917	0.1662	0.5361	0.6487	2.0
430	0.2389	0.2066	0.5444	0.6750	1.8
495	0.3000	0.2595	0.6333	0.7878	2.2
545	0.2944	0.2542	0.6667	0.7950	2.1
700	0.3139	0.2711	0.6972	0.8153	2.3
800	0.3194	0.2764	0.6972	0.8605	1.9

Similarly, the bond angles have roughly converged by 495 eV (Table 8). The angle with the largest error varies as the basis set increases: a CNO angle largest at 330 eV, a HCH angle at 430 eV, and for 494 through 800 eV the largest error is in a CNN angle. However, as we have seen before, the errors in the angles are on average smaller than 0.7°.

Figure 4 illustrates the errors in the crystal lattice vectors for RDX versus E_{cut}. As seen previously, the low kinetic energy cutoffs are inadequate to properly describe the momentum space, and therefore they yield extremely large errors. However, unlike

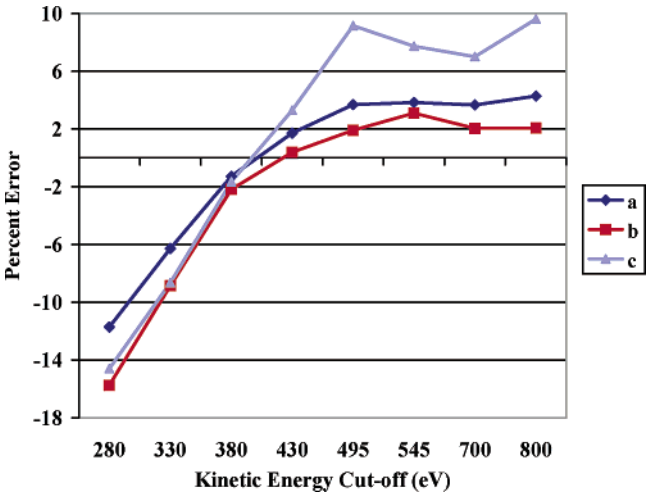

Figure 4. PW91 percent errors versus experimental lattice vectors for RDX.

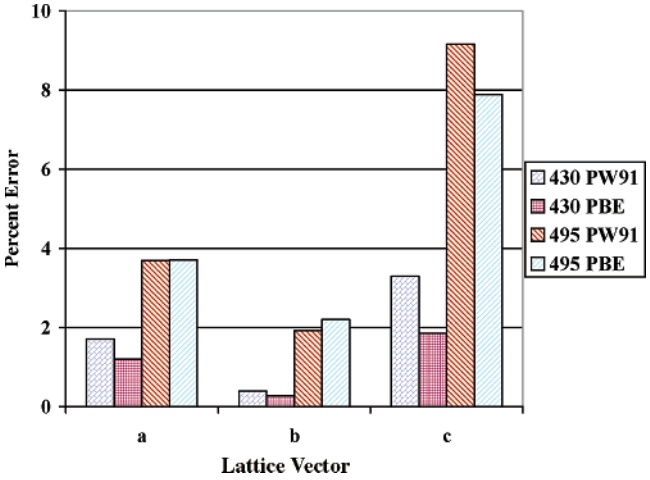

Figure 5. Percent Errors versus experimental lattice vectors for RDX.

TABLE 9: Mean, Percent Mean, Absolute Mean, Standard Deviation, and Maximum Error in Intramolecular Bond Distances versus Experiment for Various Kinetic Energy Cutoffs for the ϵ-CL20 Crystal with PW91

E_{cut} (eV)	mean (Å)	% mean	abs mean (Å)	std dev (Å)	max error (Å)
280	−0.0288	−2.0573	0.0293	0.0245	−0.090
330	−0.0137	−0.9801	0.0148	0.0149	−0.047
380	−0.0016	−0.1206	0.0033	0.0045	−0.016
430	0.0013	0.0856	0.0026	0.0040	0.013
495	0.0024	0.1582	0.0027	0.0047	0.017
545	0.0022	0.1450	0.0029	0.0050	0.018
700	0.0025	0.1672	0.0030	0.0050	0.017

HMX, even though the intramolecular bonds and angles have converged to approximately the same accuracy by 430 eV, the lattice vectors are still increasing in length for the higher E_{cut}. At 800 eV, RDX exhibits the largest error in this study, with a 9.62% error (1.03 Å) in the **c** lattice vector, and large errors in the two remaining lattice vectors with 0.57 Å and 0.24 Å errors in the **a** and **b** lattice vectors, respectively. These errors in the lattice vectors are unfortunately not limited only to the PW91 functional but are also present in the PBE functional. In Figure 5, one can observe how closely the PBE functional tracks the same errors as the PW91 functional at the 430 and 495 eV basis sets. While the PBE functional does improve marginally on the errors in the **c** lattice vector, at 495 eV there still exists a quite large approximate 8% error (0.8 Å), inconsistent with accurate calculations.

3.4. CL20. Finally we turn to ϵ-CL20, the most stable polymorph of CL20 with 144 atoms per crystal cell, which has a space group of $P2_1/n$ and experimental lattice vectors of **a** = 8.852 Å, **b** = 12.556 Å, and **c** = 13.386 Å and lattice angles of $\alpha = \gamma = 90.0°$, and $\beta = 106.82°$.[19] *k*-Point testing was done with the one (1 × 1 × 1) and four (2 × 2 × 2) *k*-point grids at 495 eV. The largest difference in lattice vectors between the two different *k*-point grids was the **b** vector at 0.19 Å (1.51%) and the smallest difference the **a** vector at 0.10 Å (1.12%), with the four *k*-point grid yielding the longer lattice vectors. However, with such a large unit cell, extensive calculations with the four *k*-point grid were computationally intractable, and therefore the calculations were performed using the one (1 × 1 × 1) *k*-point grid. In testing for convergence with kinetic energy cutoff, we ran calculations at 280, 330, 380, 430, 495, 545, and 700 eV.

For the CL20 crystal, intramolecular errors are small (Table 9), almost an order of magnitude smaller than the other crystals in this study. Maximum errors are roughly a factor of 3 smaller than those seen for the other crystals. One possible explanation

TABLE 10: Mean, Percent Mean, Absolute Mean, Standard Deviation, and Maximum Error in Intramolecular Angles versus Experiment for Various Kinetic Energy Cutoffs for the ϵ-CL20 Crystal with PW91

E_{cut} (eV)	mean (deg)	% mean	abs mean (deg)	std dev (deg)	max error (deg)
280	−0.0972	−0.0648	1.7722	2.3761	−8.1
330	0.0306	0.0377	1.1389	1.4587	5.6
380	−0.0347	−0.0251	0.4458	0.6070	2.0
430	−0.0333	−0.0262	0.1528	0.2195	−0.8
495	−0.0014	−0.0011	0.0014	0.0118	−0.1
545	0.0286	0.2311	0.1369	0.2161	1.0
700	−0.0069	−0.0058	0.0264	0.0513	−0.1

of this phenomenon is the more rigid structure of the CL20 molecule. As all calculations were initiated from the experimental crystal structure, the lack of atomic mobility restricted the molecular crystal to remain close to the starting structure. As before, intramolecular distances are converged by 495 eV.

Table 10 shows that the bond angles are also predicted more accurately for Cl20 than those of the other crystals in this study. We observe angle errors approximately 2 to 10 times smaller than in previous structures. While the errors are in general smaller than for other structures, there appears to be little convergence in the angle errors for increasing basis set size. However, with maximum errors on the order of 1° or smaller, and standard deviations of 0.22° or less for all calculations with basis sets larger than 430 eV, a small amount of fluctuation is not a serious concern.

However, for lattice vectors the trend for large errors continues, where we observe maximum **b** lattice vector error of 6.1% (0.77 Å) at 545 eV (Figure 6). Even progressing to a 700 eV E_{cut}, the **b** vector error remains large at 5.3% (0.66 Å). While the percent errors are on a par with those of nitromethane and HMX, this is deceiving as the experimental lattice vectors for CL20 are larger than those of the other two molecular crystals. Therefore the absolute errors in angstroms are larger for CL20 than for nitromethane and HMX. The disparity in the accuracy of the intramolecular distances and angles compared to the inaccuracy of the lattice vectors is most pronounced in CL20.

3.5. Band Energies. As stated previously, the initial purpose of this study was to examine the band structure of energetic materials and observe the response of the band gap (lowest unoccupied orbital minus highest occupied orbital) during compression of the crystal lattice. As we have seen, using DFT

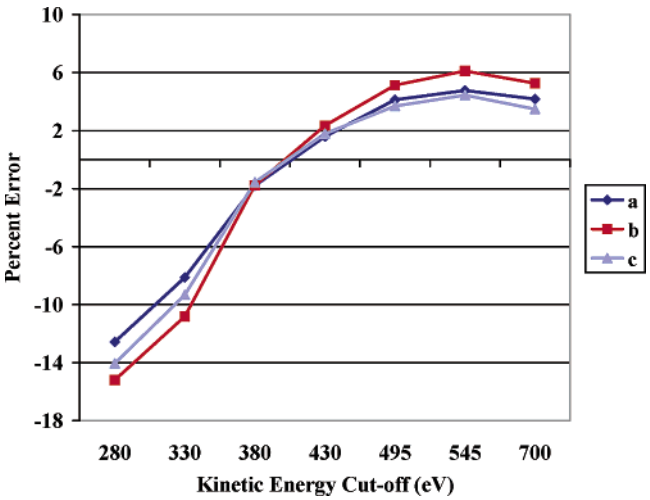

Figure 6. PW91 percent errors versus experimental lattice vectors for CL20.

TABLE 11: Band Gap Energies (eV) versus Kinetic Energy Cutoffs for the Nitromethane, HMX, RDX, and CL20 Crystals with PW91

	band gap energy (eV)			
E_{cut} (eV)	nitromethane	HMX	RDX	CL20
280	3.29	3.23	2.38	2.89
330	3.36	3.36	3.04	3.22
380	3.40	3.47	3.35	3.51
430	3.43	3.47	3.44	3.56
495	3.45	3.49	3.53	3.59
545	3.47	3.50	3.52	3.59
645	3.46			
700	3.45	3.49	3.52	3.59
800			3.50	

TABLE 12: Percent Errors in the Computed Crystal Densities versus Experiment for the Nitromethane, HMX, RDX, and CL20 Crystals with PW91

	percent error			
E_{cut} (eV)	nitromethane	HMX	RDX	CL20
495	−13.5	−10.6	−13.3	−11.8
545	−16.3	−12.5	−13.3	−13.4
700	−15.1	−10.1	−11.7	−11.8

as applied here is unsuitable for accurately predicting ground state crystal densities of molecular crystals. However, it is still of interest to observe the effect of increasing basis set size on band gap energies.

Table 11 illustrates that, similar to the trends in intramolecular parameters, band gap energies have converged by an E_{cut} of 495 eV. Once again, at low E_{cut}, the energies have not completely converged and one is required to go to larger basis sets. While the band gap energies have converged, it is impossible to predict the error due to the inaccuracies in the lattice dimensions. The band gap energies are related to the periodic potential generated by the locations of the molecules in the crystal. The apparent inadequacies in describing van der Waals interactions in the DFT potential will influence the band energies, making accurate prediction difficult.[20,21] Since it is problematic to determine the error in the band energies from the errors in the lattice vectors, using DFT to compute changes in the band energies due to compression would be imprudent. If the error is due primarily to inaccurate accounting of van der Waals forces,[22] the lack of these dispersion forces makes suspect any computed values in the low to medium pressure regime.

4. Conclusion

Using the PW91 and PBE DFT functionals, we have studied four common energetic molecular crystals, nitromethane, HMX, RDX, and CL20, with a wide range of basis sets. Intramolecular distances, angles, and band gaps are converged by E_{cut} of 430 to 495 eV. Lattice vectors, however, display large errors in the range of 0.2 Å to 1.0 Å (up to a 9.6% error) and a slower convergence on basis set size. Table 12 illustrates the impact in these large lattice vector errors on the density, where we see percent differences versus experiment of 10% or more in the computed crystalline densities. Recalling that experimentalists would prefer predictions with deviations of 1% or less, these errors in the crystal densities establish that current density functional theories are unsuitable for accurate predictions.

We tested different *k*-point spaces to determine the proper saturation level. We also compared the PW91 and PBE functional for both nitromethane and RDX. There were minimal differences between the two methods for the same basis set size. Gaussian based DFT calculations using the PBE functional were computed for nitromethane in order to test inaccuracies in plane wave basis sets. The 6-31G** basis set yielded results for cell vectors in slightly better agreement with experiment than the plane wave results with the largest E_{cut}.

We hypothesize that the error in the lattice vectors is due to a lack of van der Waals forces for nonoverlapping densities in current DFT functionals. This is supported by the fact that the molecular structures are generally in much better agreement with experiment than are the unit cell vectors, which should depend more on the effect of dispersion forces than would the structure of an isolated molecule. Inaccurate van der Waals forces cause an underestimation in the attractive forces between the molecules in the crystals and thus an overestimation in the overall lattice vectors. This deficiency could have unforeseen consequences on all molecular crystal calculations, particularly for those at low pressure, and therefore caution should be employed whenever interpreting results obtained from any solid state DFT code. To properly describe the electronic structure of the crystals, possible solutions are (1) to develop new functionals which include accurate dispersion forces for nonoverlapping or nearly overlapping densities,[23,24] (2) to employ linear response theory to calculate the frequency dependent susceptibility and use it to obtain the dispersion forces, (3) or to use perturbation theory for the intermolecular correlation and DFT for the intramolecular correlation, taking care to avoid double-counting.

Acknowledgment. Calculations were performed at the DOD High Performance Computing site at the U.S. Army Research Laboratory, Aberdeen Proving Grounds, MD. G.E.S. is supported by the NSF and the Welch Foundation.

References and Notes

(1) Hohenberg, P.; Kohn, W. *Phys. Rev. B* **1964**, *140*, 864.
(2) Rice, B. M.; Chabalowski, C. F. *J. Phys. Chem* **1997**, *101*, 8720.
(3) Reed, E. J.; Joannopoulos, J. D.; Fried, L. E. *Phys. Rev. B* **2000**, *62*, 16500.
(4) Smith, G. D.; Bharadwaj, R. K. *J. Phys. Chem. B* **1999**, *103*, 3570.
(5) Chakraborty, D.; Muller, R. P.; Dasgupta, S.; Goddard, W. A., III. *J. Phys. Chem. A* **2000**, *104*, 2261.
(6) Chakraborty, D.; Muller, R. P.; Dasgupta, S.; Goddard, W. A., III. *J. Phys. Chem. A* **2001**, *105*, 1302.
(7) Kuklja, M. M.; Kunz, A. B. *J. Appl. Phys.***1999**, *86*, 4428.
(8) Dr. Rao Surapaneni, ARDEC, Picatinny Arsenal, NJ, private communication.
(9) Perdew, J. P. In *Electronic Structures of Solids '91*; Ziesche, P., Eschrig, H., Eds.; Akademie-Verlag: Berlin, 1991.
(10) Kresse, G.; Furthmuller, J. *Vienna Ab-initio Simulation Package (VASP): The Guide*; VASP Group, Institut für Materialphysik, Universitat Wien: Sensengasse 8, A-1130 Wien, Vienna, Austria, 2003.
(11) Perdew, J. P.; Berke, K.; Ernzerhof, M. *Phys. Rev. Lett* **1996**, *77*, 3865.
(12) Vanderbilt, D. *Phys. Rev. B* **1990**, *41*, 7892.
(13) Methfessel, M.; Paxton, A. T. *Phys. Rev. B* **1989**, *40*, 3616.
(14) Frisch, M. J.; Trucks, G. W.; Schlegel, H. B.; Scuseria, G. E.; Robb, M. A.; Cheeseman, J. R.; Montgomery, J. A., Jr.; Vreven, T.; Kudin, K. N.; Burant, J. C.; Millam, J. M.; Iyengar, S. S.; Tomasi, J.; Barone, V.; Mennucci, B.; Cossi, M.; Scalmani, G.; Rega, N.; Petersson, G. A.; Nakatsuji, H.; Hada, M.; Ehara, M.; Toyota, K.; Fukuda, R.; Hasegawa, J.; Ishida, M.; Nakajima, T.; Honda, Y.; Kitao, O.; Nakai, H.; Klene, M.; Li, X.; Knox, J. E.; Hratchian, H. P.; Cross, J. B.; Adamo, C.; Jaramillo, J.; Gomperts, R.; Stratmann, R. E.; Yazyev, O.; Austin, A. J.; Cammi, R.; Pomelli, C.; Ochterski, J. W.; Ayala, P. Y.; Morokuma, K.; Voth, G. A.; Salvador, P.; Dannenberg, J. J.; Zakrzewski, V. G.; Dapprich, S.; Daniels, A. D.; Strain, M. C.; Farkas, O.; Malick, D. K.; Rabuck, A. D.; Raghavachari, K.; Foresman, J. B.; Ortiz, J. V.; Cui, Q.; Baboul, A. G.; Clifford, S.; Cioslowski, J.; Stefanov, B. B.; Liu, G.; Liashenko, A.; Piskorz, P.; Komaromi, I.; Martin, R. L.; Fox, D. J.; Keith, T.; Al-Laham, M. A.; Peng, C. Y.; Nanayakkara, A.; Challacombe, M.; Gill, P. M. W.; Johnson, B.; Chen, W.; Wong, M. W.; Gonzalez, C.; Pople, J. A. *Gaussian 03*, revision B.01; Gaussian, Inc.: Pittsburgh, PA, 2003.
(15) Binkley, J. S.; Pople, J. A.; Hehre, W. J. *J. Am. Chem. Soc*. **1980**, *102*, 939. Gordon, M. S.; Binkley, J. S.; Pople, J. A.; Pietro, W. J.; Hehre,

W. J. *J. Am. Chem. Soc*. **1983**, *104*, 2797. Hariharan, P. C.; Pople, J. A. *Theor. Chim. Acta* **1973**, *28*, 213. Francl, M. M.; Petro, W. J.; Hehre, W. J.; Binkley, J. S.; Gordon, M. S.; DeFrees, D. J.; Pople, J. A. *J. Chem. Phys*. **1982**, *77*, 3654.

(16) Trevino, S. F.; Prince, E.; Hubbard, C. R. *J. Chem. Phys.* **1980**, *73*, 2996.

(17) Choi, C. S.; Boutin, H. P. *Acta Crystallogr., Sect. B* **1970**, *26*, 123.

(18) Choi, C. S.; Prince, E. *Acta Crystallogr., Sect. B* **1972**, *28*, 2857.

(19) Nielson, A. T.; Chafin, A. P.; Christian, S. L.; Moore, D. W.; Nadler, M. P.; Nissan, R. A.; Vanderah, D. J.; Gilardi, R. D.; George, C. F.; Flippen-Anderson, J. L. *Tetrahedron* **1998**, *54*, 11793.

(20) Wu, X.; Vargas, M. C.; Nayak, S.; Lotrich, V.; Scoles, G. *J. Chem. Phys.* **2001**, *115*, 8748.

(21) Misquitta, A. J.; Jeziorski, B.; Szalewicz K. *Phys. Rev. Lett*. **2003**, *91*, 033201.

(22) Williams, H. L.; Chabalowski, C. F. *J. Phys. Chem. A* **2001**, *105*, 646.

(23) Rydberg, H.; Dion, M.; Jacobson, N.; Schröder, E.; Hyldgaard, P.; Simak, S. I.; Langreth, D. C.; Lundqvist, B. I. *Phys. Rev. Lett.* **2003**, *91*, 126402.

(24) Dion, M.; Rydberg, H.; Schröder, E.; Langreth, D. C.; Lundqvist, B. I. *Phys. Rev. Lett*. **2004**, *92*, 246401.